Journal of Power Sources 195 (2010) 1325–1332

Contents lists available at ScienceDirect

Journal of Power Sources

journal homepage: www.elsevier.com/locate/jpowsour

Preparation of high-performance polymer electrolyte nanocomposites through nanoscale silica particle dispersion

Chang Hyun Lee[a,b], Ho Bum Park[a,*], Chi Hoon Park[a], So Young Lee[a], Ju Young Kim[c], James E. McGrath[b], Young Moo Lee[a,**]

[a] School of Chemical Engineering, College of Engineering, Hanyang University, Seoul 133-791, Republic of Korea
[b] Macromolecules and Interfaces Institute and Chemistry Department, Virginia Polytechnic Institute and State University, Blacksburg, VA 24061, USA
[c] Department of Advanced Materials Engineering, Kangwon National University, Samcheok, Kangwon 245-711, Republic of Korea

ARTICLE INFO

Article history:
Received 19 June 2009
Received in revised form 13 August 2009
Accepted 26 August 2009
Available online 16 September 2009

Keywords:
Nanocomposite
Nano-level dispersion
Silica nanoparticle
Surfactant
Fuel cell

ABSTRACT

Nano-level dispersion with a minimum amount of non-porous and surface-functionalized nanoparticles is a key to tune physically a common polymer material with poor durability to a powerful material with excellent stability even under harsh fuel cell conditions. Surfactants composed of hydrophobic cores and hydrophilic outer shells are used to assist a homogenous distribution of surface-treated (hydrophilic and hydrophobic) silica nanoparticles. In particular, their effect on nanoparticle dispersion is conspicuous in polymer electrolyte nanocomposites containing hydrophilic surface-treated silica. The hydrophilic silica acts as an additional proton conductor in the acid electrolyte medium, leading to improved proton conductivity without any negative side-effects on the mechanical and chemical durability of the membrane material. The well-distributed hydrophilic silica nanoparticles are beneficial in preventing methanol permeation via compact polymer packing and in strengthening the membrane stability under hot aqueous conditions. Finally, the efficacy of the nano-level dispersion is electrochemically verified in terms of high single-cell performance and further extended life time as a result of a synergistic effect of improved proton conductivity, reduced methanol permeability and excellent hydrolytic durability.

1. Introduction

The global supply of energy is highly dependent on fossil fuels and gives rise to global warming due to the emission of greenhouse gases such as carbon dioxide [1]. There are two major options to reduce carbon dioxide emissions, namely, decreasing the energy demand or using non-carbon energy such as hydrogen. Fuel cells are emerging technologies for clean power generation in place of the combustion of fossil fuels [2]. Particularly, polymer electrolyte membrane fuel cells (PEMFCs) can be used as alternatives to internal-combustion engines in vehicles, as well as power supplies in stationary and portable applications. The fuel cells are energy-efficient, clean, and fuel-flexible (i.e., they can use hydrogen or methanol). Before PEMFC technology can gain a considerable share of the present electrical power market, however, some important issues have to be addressed. These issues include suitable materials for the bipolar plates, the electrocatalysts at the anode (fuel electrode) and the cathode (air electrode), and a proton conductive membrane, i.e., a polymer electrolyte membrane (PEM) [3]. In particular, the following properties of the PEM need to be achieved: (1) high proton conductivity; (2) low gas permeability; (3) good mechanical, chemical and thermal strength; (4) low methanol crossover, particularly for direct methanol fuel cell (DMFC); (5) lower cost. To meet these requirements, a variety of approaches have been achieved: (1) modification of sulfonated perfluorinated materials (e.g., Nafion®) [4,5]; (2) sulfonated polymers based on hydrocarbon [6–10]; (3) acid–base complexes [11]; (4) inorganic–organic hybrids or composite materials [12,13].

More recently, the incorporation of inorganic particles or fillers into polymer electrolytes for fuel cells has been a subject of growing interest because of their improved thermal stability and better water-retaining properties [14,15]. Potential candidates for inorganic particles are silica [16,17], heteropolyacid [18,19], zeolite [20], and carbon nanotubes [21]. Silica particles are of particular interest due to their ease of use, high specific area, large porous volume, large mechanical and thermal stability, and low cost. However, the primary disadvantage of the incorporation of these nanometric fillers into organic polymers is the agglomeration of fine particles, leading to the formation of non-selective cavities or uneven distribution in the polymers. A facile way to achieve good dispersion of inorganic nanoparticles within a polymer matrix is to use surface-functionalized nanoparticles (with hydrophobic or

* Corresponding author. Tel.: +82 2 2220 2338; fax: +82 2 2291 5982.
** Corresponding author. Tel.: +82 2 2220 0525; fax: +82 2 2291 5982.
E-mail addresses: badtzab@hanyang.ac.kr (H.B. Park), ymlee@hanyang.ac.kr (Y.M. Lee).

0378-7753/$ – see front matter © 2009 Elsevier B.V. All rights reserved.
doi:10.1016/j.jpowsour.2009.08.102

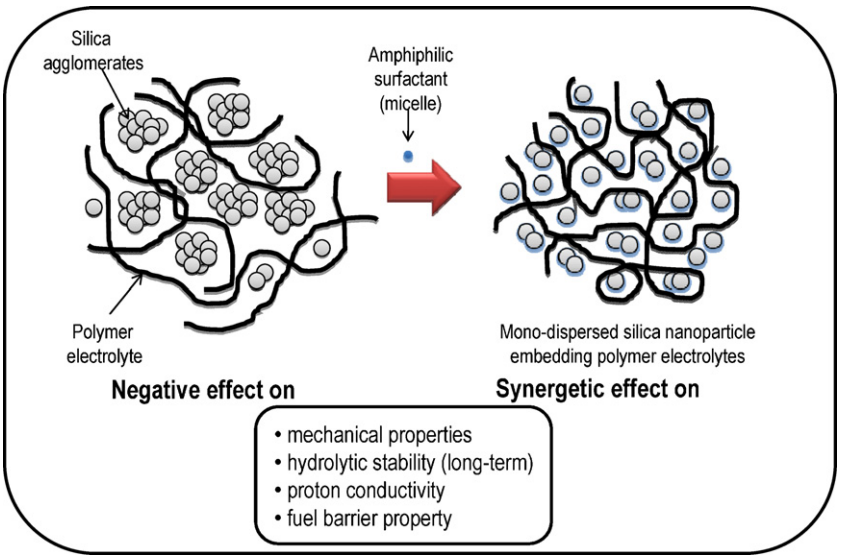

Fig. 1. Basic concept of this study: nanoscale dispersion of surface-functionalized silica particles around hydrophilic domains of polymer matrix via micelle formation using surfactants may significantly affect polymer electrolyte nanocomposite properties (chemical stability and mechanical strength) and its transport behaviour to proton and methanol molecules.

hydrophilic characteristics) for good compatibility with the polymers. The concentration of inorganic nanoparticles in a polymer is also an important determinant of the mechanical properties and free volume elements to transport ions and molecules [22,23]. Ideally, in order not to lose the advantages of polymers (e.g., processibility, ductility, and flexibility), strategies are needed to make the most of the additive effects of inorganic nanoparticles with the smallest amount of the nanoparticles. This is mainly because high concentrations of inorganic particles (as fillers) usually lead to unfavorable loss in the mechanical properties of polymer nanocomposites due to incompatibility between the inorganic particles and the organic polymers.

Here, we demonstrate a novel and facile approach to prepare highly durable polymer electrolyte nanocomposites for use under harsh fuel cell conditions by incorporating inorganic nanoparticles with surfactants, which results in well-dispersed nanoparticles incorporated in polymer electrolytes (Fig. 1). In this study, polymer electrolyte nanocomposites consist of sulfonated copolyimide (as a polymer electrolyte), fumed silica (as an inorganic nanoparticle) and non-ionic surfactant (as a dispersant) (Fig. 2). The sulfonated copolyimide (SPI, IEC = 1.9 mequiv. g^{-1}, proton conductivity = 0.07 S cm^{-1} at 90 °C and 95% RH) is selected because sulfonated polyimides generally show high proton conductivity, but they suffer from low hydrolytic stability [24,25] as compared with perfluorinated sulfonated ionomers (e.g., Nafion®). Such low hydrolytic stability is harnessed in this work to investigate the effect of the dispersion properties of inorganic nanoparticles on membrane performance and hydrolytic tolerance for accelerated testing in a short period. Two types of silica are used to study the effect of their surface properties on dispersion properties: one is hydrophilic surface-treated (Aerosil® 200, average particle size = 12 nm) and the other is hydrophobic surface-treated

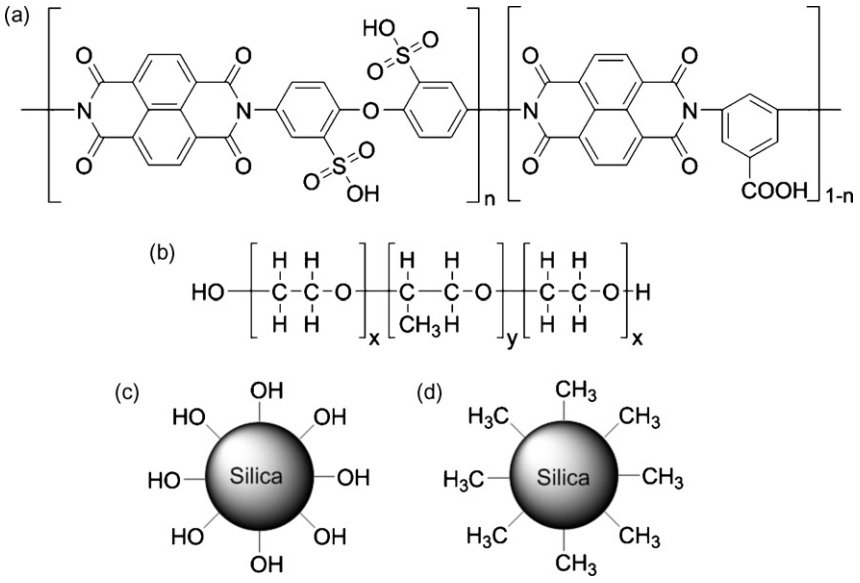

Fig. 2. Chemical structure of polymer electrolyte, non-ionic surfactant and silica nanoparticle used in this study. (a) Sulfonated copolyimide (SPI); (b) non-ionic surfactant consisting of poly(ethylene oxide)–poly(propylene oxide)–poly(ethylene oxide) triblock copolymer; (c) hydrophilic surface-treated silica (Aerosil® 200); (d) hydrophobic surface-treated silica (Aerosil® 812).

Table 1
Physicochemical properties of surfactants.

Surfactant	Composition	MW [g mol^{-1}]	PEO [mol]	Cloud point [°C]	HLB[a]	Viscosity[b] [cps]	Melting point [°C]
L31	PEO_1–PPO_{17}–PEO_1	1100	2	21–31	1–7	175	−32
L35	PEO_{11}–PPO_{16}–PEO_{11}	1900	22	78–82	18–23	375	7
L64	PEO_{13}–PPO_{30}–PEO_{13}	2900	26	58–62	12–18	850	16

[a] Hydrophilic–lipophilic balance.
[b] Measured at 25 °C.

(Aerosil® 812, average particle size = 7 nm). The amphiphilic surfactant is a PEO_x–PPO_y–PEO_x triblock copolymer (PEO: poly(ethylene oxide); PPO: poly(propylene oxide)), which is widely used in detergents, forming, lubrication, drug delivery, and membrane formation [26,27].

2. Experimental

2.1. Materials

1,4,5,8-Naphthalenic tetracarboxylic dianhydride (NTDA) as a dianhydride together with 3,5-diaminobenzoic acid (DBA) and 4,4′-diaminodiphenyl ether (ODA) as diamines were purchased (Tokyo Kasei Co., Tokyo, Japan) and used as-received. Then, ODA was converted into 4,4′-diaminodiphenyl ether-2,2′-disulfonic acid (DSODA) via direct sulfonation [28,29] using concentrated sulfuric acid (95%) and fuming sulfuric acid (SO_3, 30%) obtained from Aldrich Chemical Co. (WI, USA). Benzoic acid and triethylamine was purchased from Aldrich Chemical Co. and used without any treatment as a catalyst and an liberator of protonated amino groups, respectively. Commercial surfactants (Table 1) were received from BASF (Ludwigshafen, Germany) and used as-received. Surface-treated silica with an amorphous structure was purchased from Degussa Chemical Co. (Dusseldorf, Germany) and dried at 80 °C and 3–5 mmHg before use.

2.2. Preparation of pristine SPI as a polymer matrix for SPI/silica nanocomposites

Pristine SPI was fabricated by solution-thermal imidization using DSODA (1.6 mmol, 0.576 g), DBA (2.4 mmol, 0.365 g), and NTDA (4.0 mmol, 1.072 g). DSODA was added to 20 mL of *m*-cresol in a 250 mL three-necked round-bottomed flask equipped with a mechanical stirrer and nitrogen purge system. Then, 0.68 g of benzoic acid, 7 g of toluene, and 0.96 g of triethylamine were added to the reaction vessel. After complete dissolution, DBA was added to the vessel with stirring for at least for 1 h. Finally, NTDA powder was very carefully added to give a brownish solution. The reaction mixture was vigorously stirred under ambient conditions for a few minutes and heated at 80 and 180 °C for 4 and 24 h, respectively. Prior to cooling down to 110 °C, *m*-cresol was added to dilute the highly viscous SPI solution to 10 wt.%. The SPI solution was poured into cold acetone to eliminate un-reacted monomers or oligomers with low molecular weight. The fiber-like precipitate of SPI was collected by filtration, washing, and drying in a vacuum oven at 120 °C.

2.2.1. Fourier transform infrared (FT-IR) characteristic peaks

SPI (KBr, cm^{-1}): 1715 (symmetric υ(C=O)), 1678 (asymmetric υ (C=O)), 1407 (δ(O=C–N)), 1255 (υ(S=O)), 1088 ($\upsilon(SO_3^-)$), 918 (υ(S–OH)), and 746 (δ(O=C–N)).

2.3. Polymer electrolyte nanocomposite membrane fabrication

Polymer powder (in the ammonium sulfonated form) was dissolved in *m*-cresol (Aldrich, Milwaukee, WI) to form a 15 wt.% solution. Nanocomposite films of these materials were prepared as follows: two silica nanoparticle types (Aerosil® 200: hydrophilic silica, BET surface area = 200 ± 25 m^2 g^{-1}; Aerosil® 812: hydrophobic silica, BET surface area = 220 ± 25 m^2 g^{-1}) were dispersed in *m*-cresol that included different surfactants (L31, L35, and L64, 16 g L^{-1}). The silica/surfactant solution was then added to a polymer solution. The mixture was stirred for at least for 1 day at 150 °C. After degassing, the viscous solution was cast on a clean glass plate, and the solvent was slowly evaporated over 24 h, then dried at 80 °C for 2 h and at 180 °C for 10 h in a vacuum oven. To prepare films in the protonated form, salt-form films were treated in 1 M hydrochloric acid at room temperature for 8 h and then washed with deionized water to eliminate excess acid. Finally, the films were dried under vacuum at 160 °C before use.

2.4. Characterization

FT-IR spectra were obtained by using a Nicolet Magna IR 760 spectra ESP (Madison, WI, USA) in the range of 2000–500 cm^{-1}. An FE-SEM image was obtained with JEOL Model JSF 6340F (Tokyo, Japan). For TEM (FEI Company, Hillsboro, OR, USA) measurements, the samples were ultra-sectioned using a microtome equipped with a diamond knife, collected, and placed on a 200 mesh copper grid. The TEM micrographs were obtained with a Tecnai G2 gun-type apparatus running at an acceleration voltage of 200 kV.

Gas evolved during thermal decomposition of SPI membranes was registered at 5 °C intervals by a coupled quadruple mass spectrometer, which was equipped with electron ionization and a channeltron detector (Thermostar, Pfeiffer (Balzers) Vacuum Technology AG, Asslar, Germany). The coupling consisted of a heated quartz capillary tube that connected the TGA furnace outlet with the MS gas inlet through a pinhole diaphragm.

Water uptake (%) of pristine SPI, SPI/surfactant and SPI/silica/surfactant membranes was measured with their weight difference after soaking in deionized water at 25 °C for 24 h, as shown in Eq. (1):

$$W = \frac{W_w - W_d}{W_d} \quad (1)$$

where W_d and W_w are the weight of the dry and fully hydrated membrane coupons (4 cm × 4 cm), respectively.

The amount of free water in each membrane was determined by using differential scanning calorimeter (DSC, DSC 2010 thermal analyzer, TA instrument, New Castle, DE, USA). Prior to measurement, the membrane was fully hydrated in water at 25 °C for at least 24 h. Then, the membrane was hermetically sealed with a high volume fan. A DSC module was purged with nitrogen carrier gas (nitrogen flow rate = 200 mL min^{-1}), quenched down to −70 °C with liquid nitrogen, and then heated to +70 °C at a rate of 5 °C min^{-1}. The amount of free water was obtained using the following equation with pre-measured water uptake and the fusion enthalpy of the endothermic peak area around 0–10 °C (E_{fs}):

$$\text{Free water}\,(\%) = \frac{E_{fs}}{E_{fw}} \times \text{total water uptake}\,(\%) \quad (2)$$

$$\text{Bound water}\,(\%) = \text{total water uptake}\,(\%) - \text{free water}\,(\%) \quad (3)$$

where E_{fw} is endothermic heat of fusion for pure water (334 J g^{-1}).

The tensile strength of each membrane was measured with an Instron mechanical testing machine (INSTRON-1708, Boston, MA, USA) following the ASTM D882 procedure. The membranes were cut into rectangular strips, held between pneumatic grips, and stretched (a crosshead speed of 5 mm min^{-1}) at a controlled temperature at 25 ± 1 °C.

The ohmic resistances (R_s, Ω) of the films (size = 1 cm × 4 cm) were measured using four-point probe, alternating-current impedance spectroscopy in a thermo- and hygro-controlled chamber connected to an electrochemical interface (Solartron 1287, Solartron Analytical, Farnborough Hampshire, GU14, ONR, UK) and an impedance/gain-phase analyzer (Solartron 1260) [30]. The entire wiring system from the potentiometer to the electrode was shielded to avoid the interference of electromagnetic noise. The proton conductivity (σ, S cm^{-1}) was calculated as follows:

$$\sigma = \frac{l}{R_s \times S} \quad (4)$$

where l (cm) is the distance between the reference electrodes, and S (cm^2) is the cross-sectional area of the membrane.

Methanol permeability (P, cm^2 s^{-1}) was determined at 30 °C using a two-chamber diffusion cell. The diffusion cells consisted of two 60 mL chambers separated by a membrane coupon. One chamber contained a 10 M methanol solution (donor solution) and the other included deionized water (receiving solution). The methanol permeability (P) was calculated from a concentration gradient of methanol at the receiving solution using a gas chromatograph (Shimadtzu, GC-14B, Tokyo, Japan) equipped with a thermal conductivity detector (TCD):

$$P = \frac{V_B \times L}{C_A \times A} \times \frac{C_B(t)}{t} \times f \quad (5)$$

where V_B is the initial volume of pure deionized water in the water chamber; L is the membrane thickness; A is the membrane active area; C_A is the initial methanol concentration (10 M or ~33 wt.%) in the methanol solution chamber; $C_B(t)$ is the methanol concentration as a function of time (t); f is the conversion factor by GC calibration.

For formatting of the membrane-electrode assembly (MEA), an anode ink was prepared by homogeneously mixing 5 wt.% Nafion® ionomer solution (DE521, total acid capacity = 0.95–1.03 mequiv. g^{-1}, DuPont, USA) and Pt/Ru black (Hispec 6000, Johnson Matthey, London, UK) in a IPA–water mixture (IPA:water = 3:1, by weight). For cathode ink formation, Pt black (Hispec 1000, Johnson Matthey, London, UK) was added, instead of Pt/Ru black used for the anode ink. Each ink was spray-coated on the surfaces of pristine SPI, SPI/silica/surfactant and Nafion® 117 membranes via the catalyst-coated membrane (CCM) method, until each catalyst loading reached 3 mg cm^{-2} on both sides of a given membrane. After complete drying under ambient condition, the catalyst-coated membrane was sandwiched between carbon papers (B-2/090/Standard wet proofing carbon paper, Toray, Tokyo, Japan) that gas served as diffusion layers, without a hot pressing process.

3. Results and discussion

3.1. Nanosized inorganic particle dispersion

The amphiphilic surfactant was primarily considered as a dispersant with a hydrophobic and hydrophilic balance to prevent the unfavorable agglomeration of nanosized fine silica within the polymer electrolyte. The concentration (16 mg mL^{-1}) of surfactant (e.g., L64, x = 13 and y = 30) was usually higher than its critical micelle concentration [4.3 mg mL^{-1}, determined using a dynamic light scattering instrument (Zetasizer, Model HAS 300, Malvern, Worcestershire, UK)] in m-cresol (as solvent). This indicates that the surfactants in m-cresol exist as micelle structures consisting of hydrophobic cores (PPO segments) and hydrophilic outer shells (PEO segments), as often observed in aqueous media [31,32]. Fig. 3 shows Z-average sizes (nm, cumulates size) of surfactant micelles (L64) and a mixture of surfactant and hydrophilic surface-treated silica (Aerosil® 200) in m-cresol. The Z-average size of L64 micelles is smaller than that of Aerosil® 200 nanoparticles in m-cresol within the measured temperature range. The Z-average size of the mixture is larger than any other case, indicating that the silica nanoparticles are covered with L64 micelles, which prevents the agglomeration of silica nanoparticles even during mixing with a viscous polymer electrolyte.

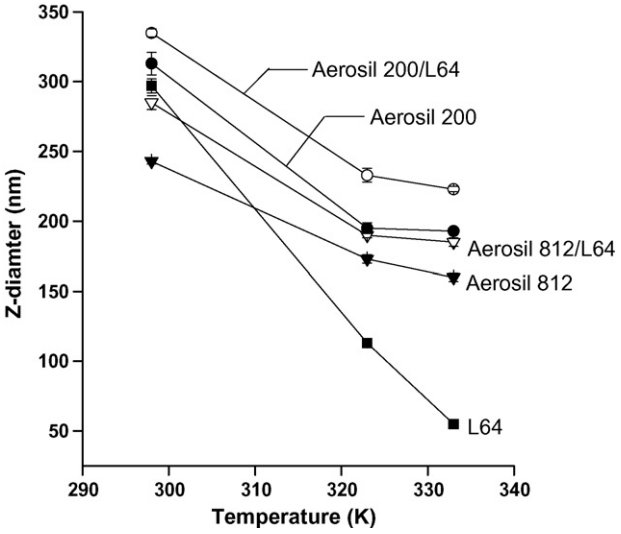

Fig. 3. Z-diameter of surfactant (L64), silica (Aerosil® 200 and Aerosil® 812), and silica/surfactant (Aerosil® 200/L64 and Aerosil® 812/L64) in m-cresol as function of temperature. Z-diameter is measured using dynamic light scattering under pH 4, which is controlled by using 0.1N HCl (standard deviation <5.1%, and polydispersity index <0.35).

The surfactants significantly contributed to the dispersion properties of silica nanoparticles in a polymer electrolyte membrane. A scanning electron microscopy (SEM) image (Fig. 4(a)) of a SPI/silica nanocomposite membrane without surfactant still shows the agglomeration of silica particles despite the use of hydrophilic surface-treated silica. In such a case, the agglomeration of fine particles leads to the formation of non-selective cavities at the interface of the particles and the polymer electrolyte, that is, it will give rise to a negative effect rather than achieving the desired dispersion. In sharp contrast, with surfactant, the SPI/silica nanocomposite does not show any large agglomerates (Fig. 4(b)), which suggests that the surfactant assists in homogeneously distributing the silica particles through the nanocomposite. Si-mapping images (white dot = silicon element) also distinctly show the dispersion state of silica in the presence and absence of surfactant. With the same surfactant, a comparison was made of the dispersion properties of silica subjected to different treatments (i.e., hydrophilic and hydrophobic surface-treated silica) by means of transmission electron microscopy (TEM). Fig. 4(c) and (d) clearly demonstrate that the hydrophilic surface-treated silica nanoparticles are much more homogeneously dispersed than the hydrophobic surface-treated silica, because the outer shells of the surfactant micelles are hydrophilic.

The surfactants seem to exist stably in the membranes without a severe leaching-out problem even under aqueous conditions, and thereby show good compatibility with the sulfonated poly-

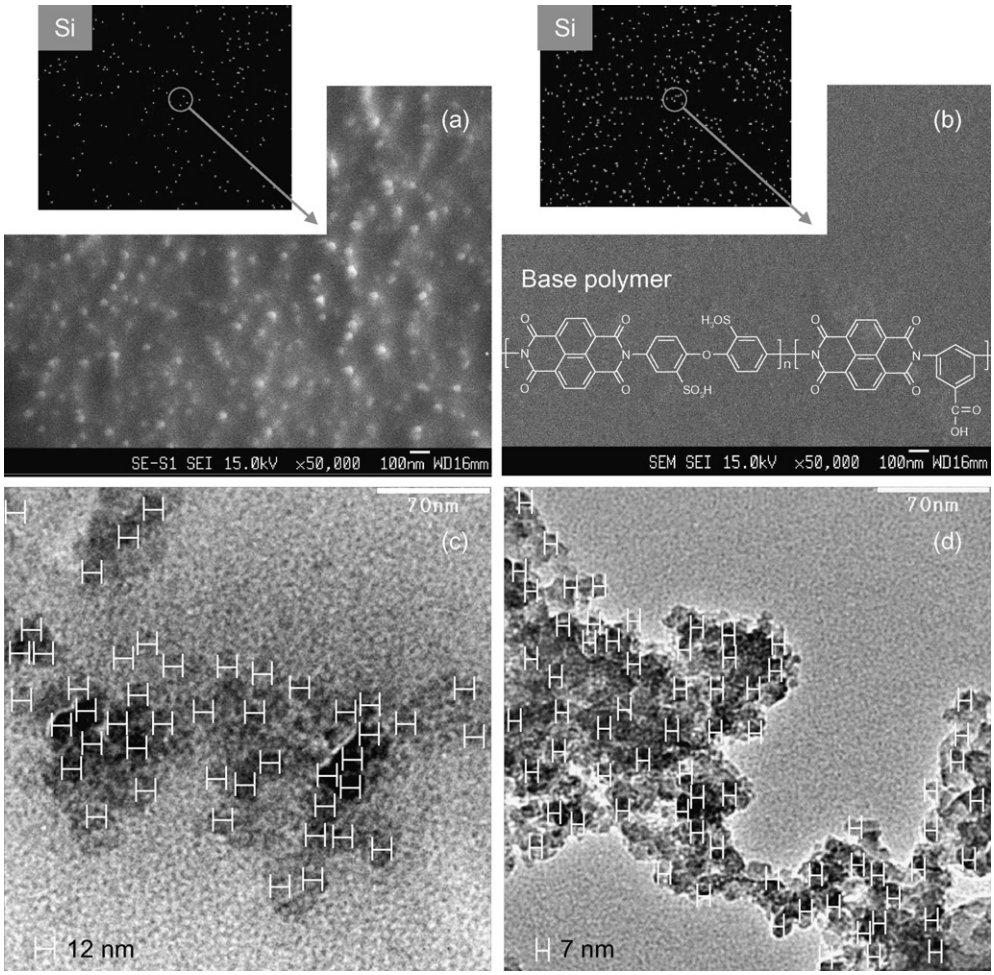

Fig. 4. FE-SEM [(a) and (b)] and TEM [(c) and (d)] images of SPI/silica nanocomposite membranes containing 1 wt.% of silica content: (a) SPI/silica without surfactant; (b) SPI/silica/surfactant (L64) (Si-mapping EDS images taken with a magnifying power of 1000); (c) SPI/silica (hydrophilic)/surfactant; (d) SPI/silica (hydrophobic)/surfactant.

mer matrix. This may be attributed to strong interaction (i.e., hydrogen bond) with SPI and silica nanoparticles. Also, a small amount of covalent bond formation between two hydroxyl groups in the surfactants and carboxylic acid groups in the SPI is verified by the corresponding FT-IR absorption peaks (1730–1735 and 1124 cm^{-1}). A comparison was made of thermal decomposition temperature (T_d) of pure surfactant (L64) and the surfactant in the sulfonated polymer using a thermo-gravimetric analysis–mass spectrometer (TGA–MS). In region II, known as a thermal desulfonation region see (Fig. 5), the additional weight loss by the evolution of carbon dioxide (CO_2) derived from L64 is observed from 150 to 350 °C only for the SPI/surfactant. The T_d value is much higher than that of pure L64 (~95 °C, measured). This means that additional bond dissociation energy is required to break the strong interaction between surfactants and the polymer matrix.

3.2. Transport properties and hydrolytic stability of polymer electrolyte nanocomposites

Fig. 6(a) shows the proton conductivity and methanol permeability of SPI/hydrophilic silica/surfactant as a function of silica content. Proton conductivity increases as the hydrophilic silica loading is increased. The hydrophilicity of the silica used in this work is due to the silanol group (–Si–OH) on the surface of the silica nanoparticles. The isoelectric point (IEP) of silica is 2 [33], at which –Si–OH groups on the silica surface exist in the neutral state. In acidic media such as a PEM (pH 0–1) [34] with a pH below the IEP of silica, –Si–OH groups are converted to the aquo state (Si–$(OH_2)^+$) [35]. That is, the silica particles play a role in an additional proton conductor and strengthen secondary hydrogen bonding with SO_3^- groups in SPI. The proton conductivity is not correlated with the water uptake of SPI/silica nanocomposite

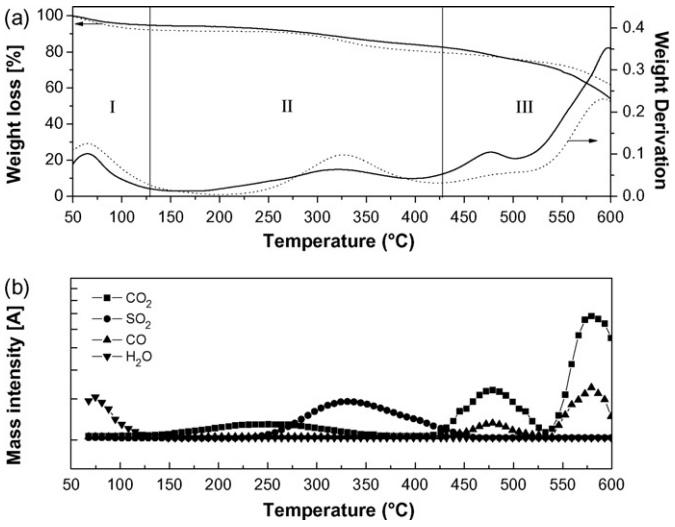

Fig. 5. (a) TGA spectra of pristine SPI (dot line) and SPI/surfactant (L64) (solid line), and (b) TGA–MS spectra of SPI/surfactant (L64).

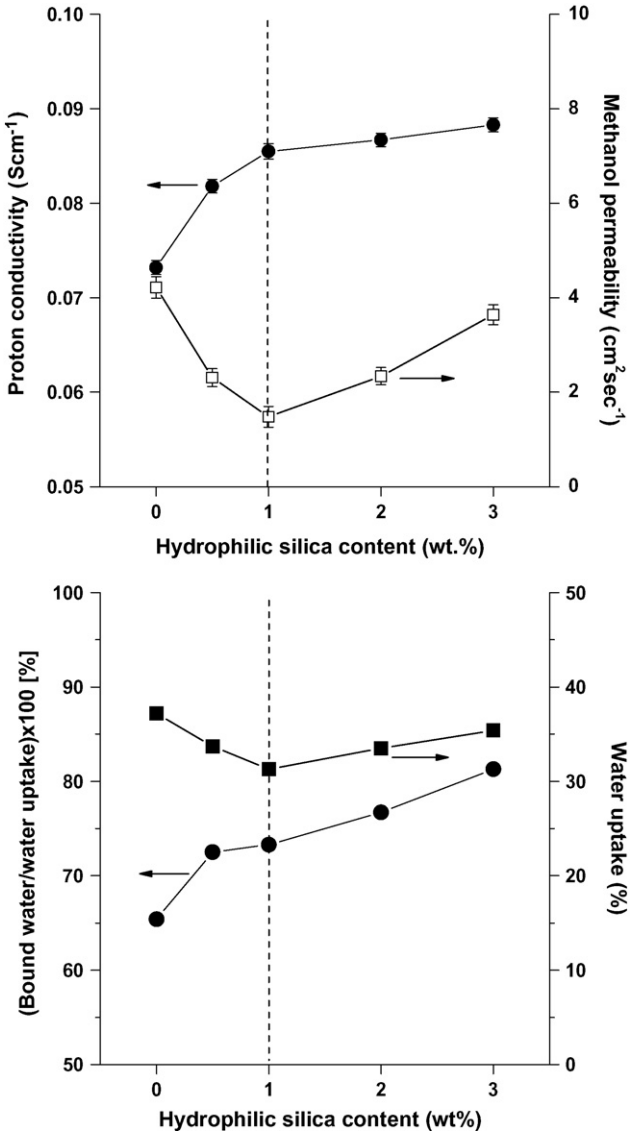

Fig. 6. (a) Proton conductivity and methanol permeability and (b) bound water/water uptake and water uptake of SPI/silica (hydrophilic)/surfactant nanocomposite membranes as function of silica content.

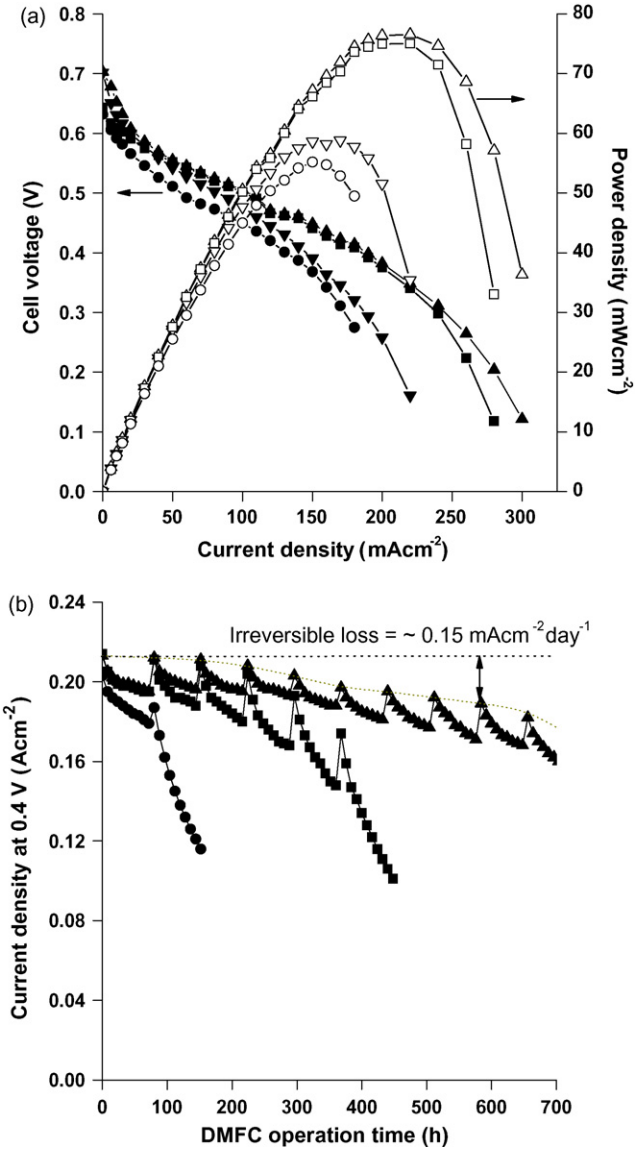

Fig. 7. (a) *V–I* and *P–I* curves of: Nafion® 117 (■); pristine SPI (●); SPI/silica (hydrophilic, 1 wt.%)/surfactant (▲); SPI/silica (hydrophobic, 1 wt.%)/surfactant (▼). The fuel cell was run at 90 °C, with the anode being fed with 1 M methanol at 1 mL min^{-1} and the cathode being fed with O_2 at 0.1 MPa and 200 mL min^{-1}. (b) Long-term DMFC performance of Nafion® 117 (■), pristine SPI (●), and SPI/silica (hydrophilic, 1 wt.%)/surfactant (▲) measured at a constant voltage (0.4 V) under same operation condition.

membranes, as shown in Fig. 6(b). On the other hand, the amount of bound water significantly affects the proton conductivity. Note that the bound water content and the proton conductivity increase as the silica particle loading is increased. Generally, the state of water in a polymer can be classified into free water and bound water [36]. Bound water can interact strongly with hydrophilic groups such as sulfonic acid or silanol groups, leading to improved proton conduction even at elevated temperatures [37]. Methanol permeability as a function of silica loading content is also quite interesting, because it decreases as the particle loading is increased at low silica particle loadings (below 1 wt.%), but above 1 wt.% the permeability increases again. At low particle loadings, the trend agrees with composite models such as the Maxwell model (i.e., as impermeable filler content increases, the penetrant permeability decreases) [38,39]. As the silica particle content is increased, however, the methanol permeability increases. Similar behaviour can be found in the gas transport behaviour of polymer nanocomposite membranes filled with impermeable inorganic fillers such as TiO_2 [40]. In the present case, silica nanoparticles began to aggregate at over 1 wt.%, which physically disrupts the efficient polymer chain packing and thereby leads to increased free volume elements for methanol permeability. In addition, as shown in Fig. 6(b), the methanol permeability is not associated with an increase in bound water, whereas the methanol permeability is strongly affected by total water uptake behaviour.

The hydrolytic stability of PEM for fuel cell applications is an important issue to ensure reliability in terms of long-term operation. Hydrocarbon-based polymer electrolyte membranes, particularly those with high proton conductivity due to a high degree of sulfonation, show low hydrolytic stability. Sulfonated polyimide itself, which is used in this work, also shows a low tolerance to hydrolytic attack compared with perfluorinated sulfonic acid ionomers (e.g., Nafion®). Actually, pristine SPI becomes brittle even within a few days after exposure in boiling water. In a previous study [28,29], by the crosslinking such SPI with various diols, the hydrolytic stability was improved, but it was not satisfactory for long-term operation in a fuel cell. Interestingly, a well-dispersed silica phase created with the aid of surfactant contributes to a

Table 2
Materials characterization of pristine SPI and SPI/silica nanocomposite membranes.

Sample	Fumed silica	Silica content [wt.%]	Water uptake [%]	$W_{bound}/W_{free} \times 100$[a] [%]	Hydrolytic stability[b] [day]	Proton conductivity [S cm^{-1}]		Tensile strength [MPa]	
						Before	After[c]	Before	After[c]
Pristine SPI	[–]	0	33.3	52.9	2.9	6.60	6.31	96.0	94.3
SPI/surfactant (L64)	[–]	0	37.2	65.4	145.8	8.19	7.79	104.3	102.8
SPI/silica/surfactant (L31)		1	35.1	56.2	>366.3	6.15	6.14	102.2	102.0
SPI/silica/surfactant (L35)	Aerosil 200	1	34.2	60.6	>366.3	7.85	7.84	103.3	103.0
SPI/silica/surfactant (L64)		0.5	33.7	72.5	>366.3	8.80	8.78	107.3	107.1
		1	31.3	73.3	>366.3	9.27	9.25	104.4	104.2
		2	33.5	76.7	>366.3	9.42	9.41	108.0	107.8
		3	35.4	81.3	>366.3	9.52	9.50	109.6	109.3
	Aerosil 812	1	28.2	60.5	>366.3	4.59	4.58	106.5	106.4

[a] W_{free} and W_{bound} indicate free water content and bound water content, respectively.
[b] The elapsed time that proton conductivity and tensile strength are not changed within 5 and 2%, respectively.
[c] Properties measured after elapsed time.

remarkable enhancement in the hydrolytic stability of the SPI/silica nanocomposite membranes, as well as in their mechanical properties (Table 2). Despite the low hydrolytic stability of pristine SPI, surprisingly there are no significant losses in proton conductivity and mechanical properties for over 1 year. Strong physical interaction (e.g., hydrogen bonding) with SPI and silica nanoparticles leads to synergetic contributions to proton conductivity and mechanical durability. This is very encouraging, because only a small quantity of silica nanoparticles (~1 wt.%) can induce highly durable PEM materials for fuel cells. Note that SPI/silica nanocomposite without surfactant or SPI/surfactant membranes still exhibit poor hydrolytic stability (Table 2). Thus, it is concluded that the key for achieving such performance is a nano-level dispersion of silica nanoparticles along the polymer electrolyte chains to restrict polymer chain mobility for undesirable degradation reactions.

3.3. Electrochemical evaluation of polymer electrolyte nanocomposites

It is important to verify the efficacy of the nano-level dispersion electrochemically via fuel cell tests (cell potential versus current density measurements). The test was performed under the desired temperature condition (90 °C) in the DMFC. For these studies, 1 M methanol solution was fed to the anode side at a rate of 1 mL min^{-1} and high purity oxygen was fed to the cathode side at a rate of 200 mL min^{-1}. Fig. 7(a) presents the current–voltage profiles for MEAs containing four different membranes: pristine SPI, SPI/silica (hydrophilic)/surfactant (L64), SPI/silica (hydrophobic)/surfactant (L64), and Nafion® 117 (as a control). The MEAs are identically prepared using the same conditions (membrane active layer = 5 cm^2; catalyst loading content = 3.0 mg cm^{-2} for anode (Pt black) and cathode (Pt–Ru black); catalyst binder content = 0.3 mg cm^{-2}). The electrochemical performance of the MEAs depends highly on both the proton conductivity and methanol permeability of each membrane. As a result, the MEA containing a SPI/silica (hydrophilic)/surfactant nanocomposite membrane shows the best single-cell performance owing to its higher proton conductivity (0.093 S cm^{-1} at 90 °C) and lower methanol permeability (1.5×10^{-7} cm^2 s^{-1} at 25 °C). The MEA with a SPI/silica (hydrophobic)/surfactant nanocomposite membrane (0.047 S cm^{-1} at 90 °C) exhibit relatively lower single-cell performance than Nafion® 117-based MEA (0.078 S cm^{-1} at 90 °C) mainly owing to the lower proton conductivity of the nanocomposite membrane, in spite of its reduced methanol permeability.

Fig. 7(b) shows the long-term stability of each single cell under an accelerated physicochemical and electrochemical degradation conditions in which DMFC operations were periodically stopped and then continued again. Remarkably, in the case of single-cell

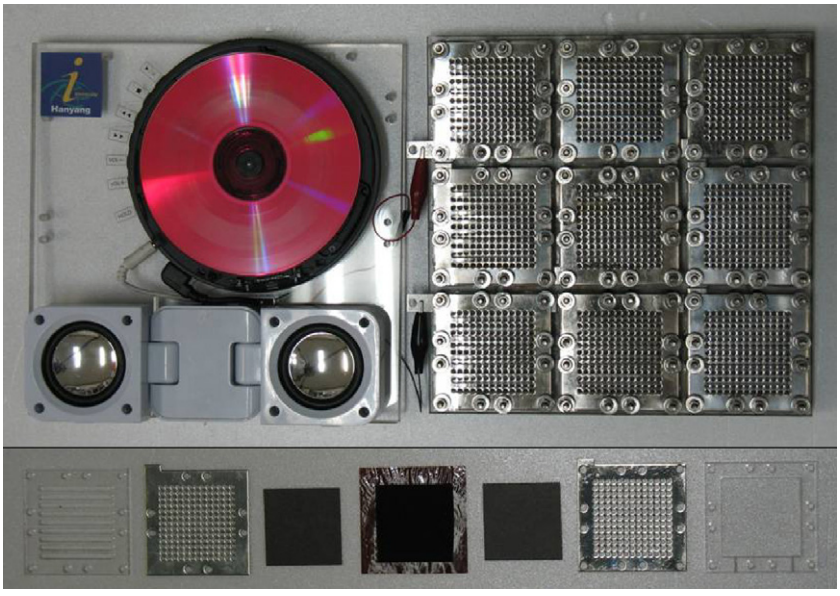

Fig. 8. Air-breathing passive DMFC system composed of nine sheets of MEAs based on SPI/silica (hydrophilic, 1 wt.%)/surfactant (L64). Methanol concentration in feed = 1 M.

performance, the SPI/silica (hydrophilic, 1 wt.%)/surfactant (L64) nanocomposite membrane shows a much longer membrane lifetime than Nafion® 117, maintaining its performance for up to 850 h with a low irreversible loss of ~0.15 mA cm^{-2} per day. Note that the pristine SPI *per se* exhibits the shortest long-term stability because of its poor hydrolytic stability.

Using the polymer electrolyte nanocomposite membrane containing 1 wt.% of hydrophilic silica and its MEA, we successfully demonstrated a parallel-typed passive DMFC stack (active layer of MEA = 20.3 cm^2, catalyst loading = 3 mg cm^{-2}, and maximum power = 1 W) consisting of a nine-sheet MEA for operating a CD player (3.0 V, 1.2 W) (Fig. 8). The DMFC stack provides sufficient dc electric power to run the device continuously for over 10 months with a 1-day-feeding cycle (reservoir volume = 180 mL) of 1 M methanol solution.

4. Conclusions

In summary, with the proper incorporation of inorganic nanoparticles, polymer electrolyte nanocomposites show higher proton conductivity, lower methanol permeability and longer membrane lifetimes. In particular, a non-ionic surfactant consisting of hydrophilic and hydrophobic segments proves very efficient in stabilizing the colloidal dispersion of silica nanoparticles in the polymer electrolytes, which makes it possible to improve the membrane performances remarkably with a relatively small quantity of inorganic nanoparticles ~1 wt.% and ~10 vol.%. The small loading of inorganic nanoparticles helps to retain the advantages of organic polymers, such as flexibility, ductility and processibility. Further studies will be aimed at optimizing the polymer electrolyte nanocomposite design by using more hydrolytic-stable polymer electrolytes [41,42], different types of surfactant (e.g., anionic or cationic surfactants), and other inorganic nanoparticles to achieve high proton conductivity and low fuel crossover (e.g., low hydrogen, oxygen and methanol permeability) while maintaining excellent chemical and thermal stability.

Acknowledgements

The authors are grateful for financial support from the Korea Foundation for International Cooperation of Science & Technology (KICOS) through a grant (K20701010356-07B0100-10610) from the Korean Ministry of Education and Science Technology (MEST).

References

[1] H.V. Storch, N. Stehr, Nature 405 (2000) 615.
[2] C.E. Health, A.G. Revfsz, Science 180 (1973) 542.
[3] B.C.H. Steele, A. Heinzel, Nature 414 (2001) 345.
[4] Z.Y. Yang, R.G. Rajendran, Angew. Chem. Int. Ed. 44 (2005) 564.
[5] E.M.W. Tsang, Z. Zhang, Z. Shi, T. Soboleva, S. Holdcroft, J. Am. Chem. Soc. 129 (2007) 15016.
[6] F. Wang, M. Hickner, Y.S. Kim, T.A. Zawodzinski, J.E. McGrath, J. Membr. Sci. 197 (2002) 231.
[7] J. Ding, C. Chuy, S. Holdcroft, Adv. Funct. Mater. 12 (2002) 389.
[8] T.B. Norsten, M.D. Guiver, J. Murphy, T. Astill, T. Navessin, S. Holdcroft, B.L. Frankamp, V.M. Rotello, J. Ding, Adv. Funct. Mater. 16 (2006) 1814.
[9] T. Yamaguchi, H. Zhou, S. Nakazawa, N. Hara, Adv. Mater. 19 (2007) 592.
[10] B. Lafitte, P. Jannasch, Adv. Funct. Mater. 17 (2007) 2823.
[11] Y.T. Hong, C.H. Lee, H.S. Park, K.A. Min, H.J. Kim, S.Y. Nam, Y.M. Lee, J. Power Sources 175 (2008) 724.
[12] C.H. Lee, S.Y. Hwang, J.Y. Sohn, H.B. Park, J.Y. Kim, Y.M. Lee, J. Power Sources 163 (2006) 339.
[13] S.L. Chen, K.Q. Xu, P. Dong, Chem. Mater. 17 (2005) 5880.
[14] L.A. Utracki, R. Simha, Macromolecules 37 (2004) 10123.
[15] M.K. Mistry, N.R. Choudhury, N.K. Dutta, R. Knott, Z. Shi, S. Holdcroft, Chem. Mater. 20 (2008) 6857.
[16] H. Li, M. Nogami, Adv. Mater. 14 (2002) 912.
[17] S. Chen, K. Xu, P. Dong, Chem. Mater. 17 (2005) 5880.
[18] Y.S. Kim, F. Wang, M. Hickner, T.A. Zawodzinski, J.E. McGrath, J. Membr. Sci. 212 (2003) 263.
[19] M.L. Ponce, L. Prado, B. Ruffmann, K. Richau, R. Mohr, S.P. Nunes, J. Membr. Sci. 217 (2003) 5.
[20] J.C. McKeen, Y.S. Yan, M.E. Davis, Chem. Mater. 20 (2008) 5122.
[21] R. Kannan, B.A. Kakade, V.K. Pillai, Angew. Chem. Int. Ed. 47 (2008) 2653.
[22] K.S. Triantafyllidis, P.C. LeBaron, I. Park, T.J. Pinnavaia, Chem. Mater. 18 (2006) 4393.
[23] Y. Zhu, B. Wang, W. Gong, L. Kong, Q. Jia, Macromolecules 39 (2006) 9441.
[24] A.L. Rusanov, Adv. Polym. Sci. 111 (1994) 115.
[25] C. Genies, R. Mercier, B. Sillion, R. Petiaud, N. Cornet, G. Gebel, M. Pineri, Polymer 42 (2001) 5097.
[26] R.S. Velichkova, D.C. Christova, Prog. Polym. Sci. 20 (1995) 819.
[27] A.V. Kabanov, E.V. Batrakova, V.Y. Alakhov, Adv. Drug Deliv. Rev. 54 (2002) 759.
[28] C.H. Lee, H.B. Park, Y.S. Chung, Y.M. Lee, B.D. Freeman, Macromolecules 39 (2006) 755.
[29] H.B. Park, C.H. Lee, J.Y. Sohn, Y.M. Lee, B.D. Freeman, H.J. Kim, J. Membr. Sci. 285 (2006) 432.
[30] C.H. Lee, H.B. Park, Y.M. Lee, R.D. Lee, Ind. Eng. Chem. Res. 44 (2005) 7617.
[31] C. Price, Pure Appl. Chem. 55 (1983) 1563.
[32] L. Yang, P. Alexandridis, D.C. Steytler, M.J. Kositza, J.F. Holzwarth, Langmuir 16 (2000) 8555.
[33] Z.P. Li, B.H. Liu, K. Arai, S. Suda, J. Electrochem. Soc. 150 (2003) A868.
[34] B.P. Binks, S.O. Lumsdon, Phys. Chem. Chem. Phys. 1 (1999) 3007.
[35] R.J. Hunter, Introduction to Modern Colloid Science, Oxford Science Publication, Oxford University Press, 1993.
[36] M.S. Jhon, J.D. Andrade, J. Biomed. Mater. Res. 7 (1973) 509.
[37] S. Gottesfeld, T.A. Zawodzinski, R.C. Alkire, H. Gerischer, D.M. Kolb, C.W. Tobias (Eds.), Advances in Electrochemical Science and Engineering, Wiley-VCH, Weinheim, Germany, 1997, p. 251.
[38] R.M. Barrer, J.A. Barrie, N.K. Raman, Polymer 3 (1962) 605.
[39] J. Qiu, J.M. Zheng, K.V. Peinemann, Macromolecules 39 (2006) 4093.
[40] S. Matteucci, V.A. Kusuma, D. Sanders, S. Swinnea, B.D. Freeman, J. Membr. Sci. 307 (2008) 196.
[41] M. Sankir, Y.S. Kim, B.S. Pivovar, J.E. McGrath, J. Membr. Sci. 299 (2007) 8.
[42] H.S. Lee, A. Roy, O. Lane, S. Dunn, J.E. McGrath, Polymer 49 (2008) 715.